Heterogeneous Catalysis

DOI: 10.1002/anie.200903907

Maximizing the Localized Relaxation: The Origin of the Outstanding Oxygen Storage Capacity of κ-$Ce_2Zr_2O_8$**

Hai-Feng Wang, Yang-Long Guo, Guan-Zhong Lu, and P. Hu**

Understanding how a metal oxide structure affects its redox properties in terms of oxygen vacancy formation is of importance for rational design of new materials.[1–4] To this end, the investigation of ceria (CeO_2)-based materials is desirable because they are used in a variety of applications in which oxygen vacancies in the solids are vital.[5–11] For example, ceria-based materials can act as an oxygen buffer in automobile three-way catalysts owing to their high oxygen storage capacity (OSC).[5] Recently, a CeO_2–ZrO_2 composite oxide phase, assigned as κ-$Ce_2Zr_2O_8$, has been reported to have excellent oxygen storage/release properties, with a cerium efficiency[12] as high as 89%.[13–15] However, there remain some unexplained puzzles in the system, and more importantly the origin of such a high OSC is still unknown. Herein, we report an investigation on the OSC of κ-$Ce_2Zr_2O_8$ using first-principles calculations that aim to explain the structure effect on its redox properties.

Among all the ceria-based materials, $Ce_{1-x}Zr_xO_2$ solid solutions have been most widely used owing to their high OSC performance.[8–11] The unusual features of κ-$Ce_2Zr_2O_8$ can be summarized as follows: Firstly, the OSC mentioned above (89%) is astonishingly high considering that the cerium efficiency of pure ceria is only about 2%, and other $Ce_{1-x}Zr_xO_2$ systems generally have cerium efficiencies of less than 50%.[16] Secondly, a similar phase to κ-$Ce_2Zr_2O_8$, assigned as t-$Ce_2Zr_2O_8$, has the same stoichiometry to that of κ-$Ce_2Zr_2O_8$ but a much lower OSC (52%).[17,18] Thirdly, the oxygen vacancies in κ-$Ce_2Zr_2O_8$ were found to be in unusual positions. κ-$Ce_2Zr_2O_8$ possesses an ordered cubic structure (Figure 1a),[13–15] with a 96-atom unit cell consisting of 16 Ce^{4+}, 16 Zr^{4+}, and 64 O^{2-} ions. Both Zr^{4+} and Ce^{4+} ions are eight-coordinate, and the 64 oxygen ions can be subclassified as 8 O_a and 8 O_b (coordinated with four Ce^{4+} and four Zr^{4+}, respectively), and 48 O_c atoms that bond directly to 2 Ce^{4+} and 2 Zr^{4+} ions. X-ray adsorption fine structure (XAFS) and X-ray diffraction (XRD) analyses showed that under the reducing conditions, the oxygen vacancy forms at O_b (Figure 1b).[13,19] This result appears to contradict chemical intuition: As Zr^{4+} is considered to be irreducible, there is no proper atomic orbital in Zr^{4+} to accommodate the two excess electrons left after removing O_b, thus hindering the rupture of Zr^{4+}–O^{2-} bonds; furthermore, the binding strength of Zr^{4+}–O^{2-} is usually stronger than Ce^{4+}–O^{2-}. Why then does the oxygen vacancy form at the site O_b?

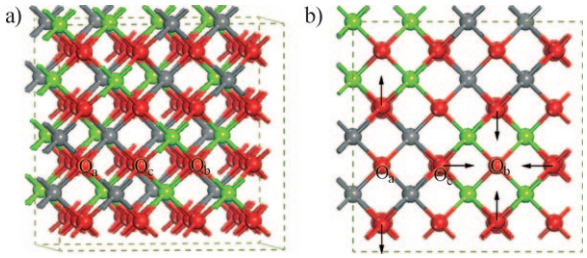

Figure 1. a) Unit cell of fluorite κ-$Ce_2Zr_2O_8$, which contains 64 O^{2-} (red), 16 Ce^{4+} (gray), and 16 Zr^{4+} (green). b) Optimized κ-$Ce_2Zr_2O_8$ structure viewed along [001]. The oxygen ions are classified into three groups: O_a, coordinated by four Ce^{4+}; O_b, coordinated by four Zr^{4+}; and O_c, coordinated by two Ce^{4+} and two Zr^{4+}. The arrows indicate the directions of forces due to the electrostatic interaction difference between Zr–O and Ce–O if O_b is removed.

Herein, we investigate the oxygen vacancy formation in κ-$Ce_2Zr_2O_8$ using density functional calculations to uncover the origin of the high OSC of κ-$Ce_2Zr_2O_8$. The calculations were performed with the GGA-PW91 functional using the VASP code.[20] To properly describe the behavior of the cerium 4f electrons, the on-site Coulomb correction was included; that is, DFT + U.[21,22] (Calculation details are given in the Supporting Information).

We calculated oxygen vacancy formation at O_a, O_b, and O_c. In the optimized κ-$Ce_2Zr_2O_8$ structure (Figure 1b), all the ions remain almost at the ideal positions with the exception of O_c, which moves slightly towards the two Zr^{4+} ions. When O_b is removed, the corresponding oxygen vacancy formation energy was calculated to be as low as 0.02 eV (0.01 eV from PBE + U). Interestingly, when the O_c is removed, a simple optimization based on the conjugate-gradient algorithm results in the nearest O_b atom automatically diffusing into the vacant O_c site, and consequently the oxygen vacancy actually forms at the O_b site. Similarly, when O_a is removed, the nearest O_c atom diffuses into the O_a site, and O_b moves to

[*] H.-F. Wang, Prof. Y.-L. Guo, Prof. G.-Z. Lu
Research Institute of Industrial Catalysis
East China University of Science & Technology
Shanghai, 200237 (China)
E-mail: gzlu@ecust.edu.cn
Prof. P. Hu
School of Chemistry and Chemical Engineering
The Queen's University of Belfast
Belfast, BT9 5AG (UK)
Fax: (+44) 28-9097-4687
E-mail: p.hu@qub.ac.uk

[**] This work is financially supported by National Basic Research Program (2004CB719500), International Science and Technology Cooperation Program (2006DFA42740), and the 111 Project (B08021).

Supporting information for this article is available on the WWW under http://dx.doi.org/10.1002/anie.200903907.

the O_c site. Thus, it is clear that in the reduction of κ-$Ce_2Zr_2O_8$, the oxygen vacancy is favored to form at the O_b site, which is consistent with the experimental results.[13,19]

We have previously shown that the oxygen vacancy formation energy consists of two contributions, the bond energy (E_{bond}) and the structural relaxation energy (E_{relax}), where E_{bond} is the energy needed to remove the oxygen atom into the gas phase with respect to the energy of half an O_2 with the geometric structure fixed, and E_{relax} is the energy gain from the fixed geometry in the presence of an oxygen vacancy to the relaxed structure.[23] Herein, we analyzed both contributions in κ-$Ce_2Zr_2O_8$ to understand why oxygen vacancy is favored to form at the O_b site.

To estimate the bond energy, E_{bond} values for O_a, O_b, and O_c with the surrounding ions were calculated (Table 1). It is clear that the weakest bond strength with the surrounding ions is that of O_b. This result is unexpected, considering that the Zr^{4+}–O^{2-} bond in ZrO_2 is generally stronger than Ce^{4+}–O^{2-} in CeO_2. Therefore, we investigated the local structure of O_b. First, the Zr^{4+} ion is held in the ideal crystal position of the fluorite structure, and consequently the bond distance between O_b and the nearest Zr^{4+} ion is 2.305 Å, which is longer than the value (2.195 Å) of the cubic ZrO_2, resulting in the noticeable decrease of the bond strength of Zr^{4+}–O^{2-}. Second, it can be seen that in the optimized κ-$Ce_2Zr_2O_8$ structure (Figure 1b), O_c moves towards the two nearest Zr^{4+} and O_b atoms owing to the stronger electrostatic attraction between Zr^{4+}–O^{2-} relative to Ce^{4+}–O^{2-} at the same bond distance. As a result, the distance between O_b and O_c is shortened, and the electrostatic repulsion between them is increased, leading to a weakening of the bond strength of O_b with its surrounding ions. To obtain quantitative bond strengths related to the electrostatic interactions, the Madelung potentials at the O_a, O_b, and O_c sites were calculated from the Ewald summation using formal charges ($V^{form} = +4$ for Zr and Ce, and −2 for O), as well as Bader charges from self-consistent PW91 + U calculation (Table 1). It can be seen that the Madelung potentials are in the same order as the bond energy terms at the O_a, O_b, and O_c sites; at the O_b site, the Madelung potential is the smallest, confirming that the bond strength of O_b is the weakest.

Once an oxygen atom is removed from the oxide matrix, the surrounding O^{2-} ions near the vacancy will relax towards the vacancy to compensate the missing bonds and gain in relaxation energy. Upon removing O_b, a large relaxation energy of 4.89 eV is gained to facilitate the O_b vacancy formation. Interestingly, the relaxation energy mainly depends on the local movements of all the six nearest-neighbor O_c ions, which move significantly towards the vacant O_b site and compensate the four missing Zr–O bonds (Figure 2a).

Table 1: Madelung potentials V^{form} and V^{PW91} and calculated E_{bond} values at the O_a, O_b, and O_c sites.

	O_a	O_b	O_c
V^{PW91} [V][a]	14.10	13.16	13.71
V^{form} [V][b]	23.88	19.98	21.96
E_{bond} [eV]	5.30	4.91	5.27

[a] Calculated from the formal charges of ions (+4 for Zr and Ce and −2 for O). [b] Obtained from the Bader charges (O: −1.24; Zr: +2.59; Ce: +2.38).

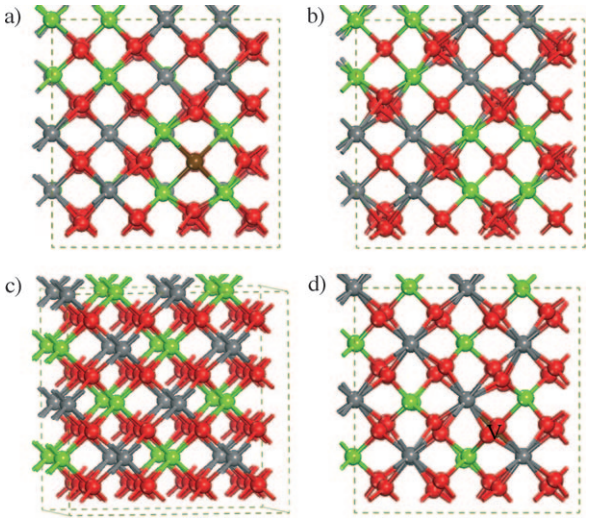

Figure 2. a) View along [001] of the optimized κ-$Ce_2Zr_2O_8$ structure in the presence of an oxygen vacancy (brown sphere). Around the oxygen atom vacancy, the six nearest-neighbor O_c atoms move towards the vacancy to give the relaxation energy. It should be noted that two of the six O_c atoms are either above or below the vacancy and not shown for clarity. b) The optimized structure of $Ce_2Zr_2O_7$ generated by removing all the eight O_b from κ-$Ce_2Zr_2O_8$. c) The optimized 96-atom bulk structure of t-$Ce_2Zr_2O_8$. d) The optimized structure of t-$Ce_2Zr_2O_8$ in the presence of an oxygen vacancy.

The remarkable displacements of O_c towards O_b are due to two factors: O_c is bonded directly with $2\,Zr^{4+}$ and $2\,Ce^{4+}$ ions, and thus there is a force pushing O_c towards the $2\,Zr^{4+}$ ions owing to the stronger electrostatic force of Zr^{4+}–O^{2-} compared to Ce^{4+}–O^{2-} in the presence of the O_b vacancy; and the smaller radius of Zr^{4+} relative to Ce^{4+} provides more space to accommodate the approaching O_c atom. However, if O_a is removed, the six nearest-neighbor O_c ions, in contrast to the case of O_b, cannot efficiently move towards the vacant O_a site because of the forces exerted on O_c in the opposite direction against their movements (Figure 1b). Similarly, for the removal of O_c, the four nearest-neighbor O_c, one O_a, and one O_b cannot move very much to provide sufficient structural relaxation, because there are no effective forces exerted on each of these six O^{2-} ions in the direction towards O_c due to their nearly symmetric bonding environments with respect to the O_c site (Figure 1b). To compare the local relaxation energy of forming an oxygen vacancy at the O_b site with those at the sites of O_a and O_c, we calculated the local relaxation energies by fixing all the ions except the six nearest-neighbor O^{2-} ions and the four nearest-neighbor cations around the vacancy site, giving values of 0.40 eV, 4.11 eV, and 2.50 eV for O_a, O_b, and O_c, respectively. Three striking features can be seen from this result. First, it shows that the relaxation is indeed largely local in the presence of

the O_b vacancy; the local relaxation energy (4.11 eV) accounts for about 85% of the total relaxation energy (4.98 eV). Second, the local relaxation is much larger at O_b (4.11 eV) than those at O_a and O_c (0.40 eV and 2.50 eV, respectively). Third, considering the small differences (ca. 0.4 eV) between the bond energy term of O_b and those of O_a/O_c (Table 1), the local relaxation differences (more than 1.61 eV) are much larger. This result suggests that the structural relaxation should be a dominating term in determining why oxygen vacancy is favored at the O_b site.

To further understand the outstanding OSC of κ-$Ce_2Zr_2O_8$, it is worth discussing the electronic structure in the system, namely the fate of the two excess electrons when O_b is removed. By examination of the projected density of state (PDOS) (Figure 3a) of κ-$Ce_2Zr_2O_8$ in the presence of an oxygen vacancy at the O_b site, we found that a very sharp 4f gap state for cerium appears at 1.40 eV above the top of the valence band; integrating this occupied 4f peak gives 1.98 e. This result shows that Zr^{4+} is indeed not reduced. Moreover, in conjunction with the isosurface plot of partial charge density of the gap states (Figure 3b), it can be seen that the two excess electrons localize separately in the 4f orbitals of the two second-nearest-neighbor Ce^{4+} cations. The separation of the excess 4f electrons in the second-nearest-neighbor cerium ions may be a general phenomenon in stabilizing defective CeO_2-based materials, considering that the two excess electrons in the pure bulk CeO_2, with an oxygen vacancy in a 96-atom supercell, was also found to localize separately at the two second-nearest-neighbor Ce^{4+} ions (Figure 3c), together with our previous work[24] and that of Ganduglia-Pirovano et al.[25] in which the localizations of the two excess 4f electrons on the second-nearest-neighbor cerium ions on defective CeO_2(111) were found to be the most stable.

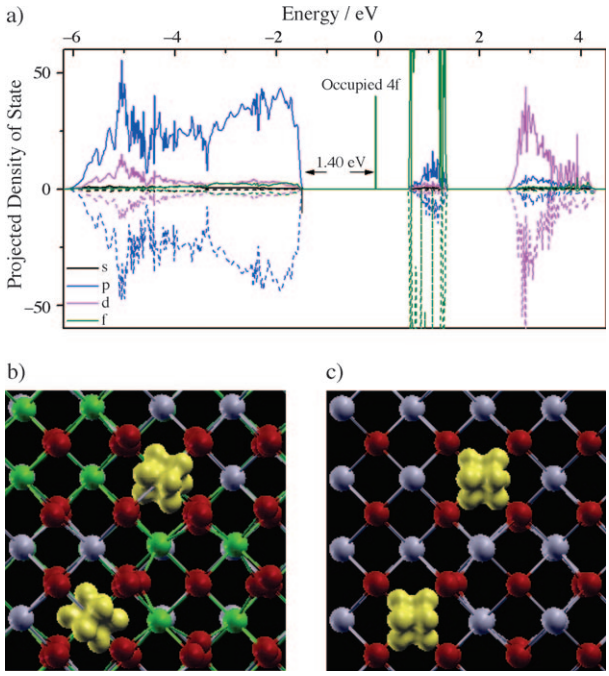

Figure 3. a) The projected density of states of defective κ-$Ce_2Zr_2O_8$. b,c) Isosurface plots of partial charge density of the gap states of κ-$Ce_2Zr_2O_8$ (b) and bulk CeO_2 (c) in the presence of an oxygen atom vacancy. Ce blue, Zr green, O red. In both cases, the two excess electrons in the presence of the oxygen vacancy are localized in the 4f orbital (yellow) of the two second-nearest-neighbor Ce^{4+} ions, thus forming two Ce^{3+} ions.

It should be pointed out that for the 96-atom supercell of κ-$Ce_2Zr_2O_8$, at most eight oxygen atoms can theoretically be removed if complete reduction is achieved ($16\,CeO_2{\cdot}16\,ZrO_2 \rightarrow 8\,Ce_2O_3{\cdot}16\,ZrO_2 + 4\,O_2$). To reveal further the origin of the high OSC of κ-$Ce_2Zr_2O_8$, we calculated the oxygen vacancy formation by removing the eight O_b atoms in the 96-atom supercell; the average oxygen vacancy formation energy was found to be very low (0.72 eV). To directly compare with κ-$Ce_2Ze_2O_8$, we also calculated a 96-atom supercell of t-$Ce_2Ze_2O_8$ containing 16 primitive cells. It was found that a low energy (0.25 eV) is needed to remove an oxygen atom from t-$Ce_2Ze_2O_8$. However, there is a significant difference between κ-$Ce_2Zr_2O_8$ and t-$Ce_2Zr_2O_8$: The average formation energy of removing eight oxygen atoms in the 96-atom supercell of t-$Ce_2Ze_2O_8$ was calculated to be 2.09 eV, which is much higher than the corresponding value (0.72 eV) in κ-$Ce_2Ze_2O_8$. This is consistent with the experimental results[13] that κ-$Ce_2Ze_2O_8$ phase possesses 89% cerium efficiency, whereas t-$Ce_2Ze_2O_8$ has an efficiency of 52%.

The major difference between t-$Ce_2Zr_2O_8$ and κ-$Ce_2Zr_2O_8$ therefore lies in the removal of eight oxygen atoms in the 96-atom supercells. Why does this difference exist although they have the same stoichiometry and similar structures? This question can be understood from the structural relaxation pattern in these two systems. As discussed above, the strong relaxation energy gained from the displacements of the surrounding oxygen ions is responsible for the low oxygen vacancy formation at the O_b site in κ-$Ce_2Ze_2O_8$, and the structural relaxation is largely localized in the six nearest-neighbor O_c ions around the O_b vacancy. In contrast, as a single oxygen atom is removed in t-$Ce_2Ze_2O_8$, the structural relaxation involves the displacements of almost all the O^{2-} ions in the t-$Ce_2Ze_2O_8$ supercell. The relaxation pattern (Figure 2d) shows a delocalization that is different from the localized relaxation nature in κ-$Ce_2Ze_2O_8$ (Figure 2a). It is thus clear that although the energy costs for creating single oxygen vacancy in both phases are not very dissimilar, the origins of the energies are quite different: In κ-$Ce_2Ze_2O_8$, each of the first-neighbor O_c ions near the vacancy moves considerably, and this local structural relaxation contributes mainly to the energy, whilst in t-$Ce_2Ze_2O_8$, it is the result of the relaxation of all the O^{2-} ions.

When eight oxygen atoms are removed in both systems, this effect of localized versus delocalized relaxation is magnified: In the 96-atom unit cell of κ-$Ce_2Ze_2O_8$, each of the eight O_b ions has its own six nearest-neighbor O_c ions; namely, every O_c belongs exclusively to a specific O_b and is not shared by any other O_b atoms. Consequently, when the eight O_b atoms are removed, their nearest-neighbor O_c ions are relaxed almost independently (see the corresponding relaxation pattern in Figure 2b). Upon removing eight oxygen atoms from t-$Ce_2Ze_2O_8$, the strong share of the

structural relaxations owing to the delocalization leads to a much higher average oxygen vacancy formation energy.

We are now in a position to address the relationship between the structure and the OSC of CeO_2-ZrO_2 composite oxides and discuss some implications of our results for rational design of new OSC materials. The structure of κ-$Ce_2Ze_2O_8$ has the following features, which are essential for its high OSC: First, the structural relaxation accompanying the removal of O_b is largely localized. Second, each local structure around O_b vacancy is such that all the six nearest-neighbor O_c move considerably, which can be considered as a local relaxation unit, and the large local relaxation is reached. Third, the number of nearly independent local relaxation units is maximized in the solid. To achieve such a structure, two conditions are required: a) the ratio of Zr/Ce in $Ce_{1-x}Zr_xO_2$ solid solutions should be close to unity; that is, the doped zirconium concentration reaches 50%; and b) the arrangement of Ce^{4+} and Zr^{4+} cations should be ordered and homogenous, which ensures the largest probability of existence of O_b and its exclusive O_c atoms. Thus, if a doped metal M can homogeneously mix with CeO_2 to form a stable κ-phase fluorite structure, κ-$Ce_{1-x}M_xO_2$, and can provide large relaxation similar to Zr^{4+}, we can expect that M may be a good dopant candidate for the new OSC material.

In summary, this work is the first attempt to pin down the key properties underlying the outstanding OSC of κ-$Ce_2Zr_2O_8$ at the atomic level using first-principles calculations. In κ-$Ce_2Zr_2O_8$, the structural relaxation plays a key role in determining the oxygen vacancy formation energy, which is largely localized, forming an independent local relaxation unit consisting of the six nearest-neighbor O_c ions with an O_b vacancy. Maximization of both the local relaxation and the number of local relaxation units plays a crucial role for the high OSC of κ-$Ce_2Zr_2O_8$.

Received: July 16, 2009
Published online: September 28, 2009

Keywords: cerium oxide · density functional calculations · oxygen storage · site vacancies · solid-state structures

[1] M. V. Ganduglia-Pirovano, A. Hofmann, J. Sauer, *Surf. Sci. Rep.* **2007**, *62*, 219.
[2] a) C. Di Valentin, G. Pacchioni, A. Selloni, *Phys. Rev. Lett.* **2006**, *97*, 166803; b) J. Carrasco, N. Lopez, F. Illas, *Phys. Rev. Lett.* **2004**, *93*, 225502.
[3] E. Perry Murray, T. Tsai, S. A. Barnett, *Nature* **1999**, *400*, 649.
[4] D. A. Andersson, S. I. Simak, N. V. Skorodumova, I. A. Abrikosov, B. Johansson, *Proc. Natl. Acad. Sci. USA* **2006**, *103*, 3518.
[5] A. Trovarelli, *Catalysis by Ceria and Related Materials*, Imperial College Press, UK, **2002**.
[6] S. Park, J. M. Vohs, R. J. Gorte, *Nature* **2000**, *404*, 265; G. A. Deluga, J. R. Salge, L. D. Schmidt, X. E. Verykios, *Science* **2004**, *303*, 993; F. Esch, S. Fabris, L. Zhou, T. Montini, C. Africh, P. Fornasiero, G. Comelli, R. Rosei, *Science* **2005**, *309*, 752.
[7] a) Q. Fu, H. Saltsburg, M. Flytzani-Stephanopoulos, *Science* **2003**, *301*, 935; b) Z. P. Liu, S. J. Jenkins, D. A. King, *Phys. Rev. Lett.* **2005**, *94*, 196102.
[8] J. Kaspar, P. Fornasiero, M. Graziani, *Catal. Today* **1999**, *50*, 285.
[9] M. Boaro, A. Trovarelli, J. H. Hwang, T. O. Mason, *Solid State Ionics* **2002**, *147*, 85.
[10] P. Fornasiero, R. Dimonte, G. R. Rao, J. Kaspar, S. Meriani, A. Trovarelli, M. Graziani, *J. Catal.* **1995**, *151*, 168.
[11] J. A. Rodriguez, J. C. Hanson, J. Y. Kim, G. Liu, A. Iglesias-Juez, M. Fernandez-Garcia, *J. Phys. Chem. B* **2003**, *107*, 3535.
[12] Cerium efficiency is defined as the ratio of cerium(III) ion content in the cerium-containing material under typical reduction conditions relative to the total cerium content; that is, $[Ce^{3+}]/([Ce^{3+}]+[Ce^{4+}])$.
[13] T. Yamamoto, A. Suzuki, Y. Nagai et al., *Angew. Chem.* **2007**, *119*, 9413; *Angew. Chem. Int. Ed.* **2007**, *46*, 9253.
[14] A. Suda, Y. Ukyo, H. Sobukawa, M. Sugiura, *J. Ceram. Soc. Jpn.* **2002**, *110*, 126.
[15] H. Kishimoto, T. Omata, S. Otsuka-Yao-Matsuo, K. Ueda, H. Hosono, H. Kawazoe, *J. Alloys Compd.* **2000**, *312*, 94.
[16] M. Sugiura, *Catal. Surv. Asia* **2003**, *7*, 77.
[17] Y. Nagai, T. Yamamoto, T. Tanaka, S. Yoshida, T. Nonaka, T. Okamoto, A. Suda, M. Sugiura, *Catal. Today* **2002**, *74*, 225.
[18] S. Lemaux, A. Bensaddik, A. M. J. Van der Eerden, J. H. Bitter, D. C. Koningsberger, *J. Phys. Chem. B* **2001**, *105*, 4810.
[19] T. Sasaki, Y. Ukyo, K. Kuroda, S. Arai, S. Muto, H. Saka, *J. Ceram. Soc. Jpn.* **2004**, *112*, 440.
[20] a) G. Kresse, J. Furthmuller, *Comp. Mater. Sci.* **1996**, *6*, 15; b) G. Kresse, J. Hafner, *Phys. Rev. B* **1994**, *49*, 14251.
[21] S. Fabris, G. Vicario, G. Balducci, S. De Gironcoli, S. Baroni, *J. Phys. Chem. B* **2005**, *109*, 22860.
[22] a) M. Nolan, S. C. Parker, G. W. Watson, *Surf. Sci.* **2005**, *595*, 223; b) M. Nolan, S. Grigoleit, D. C. Sayle, S. C. Parker, G. W. Watson, *Surf. Sci.* **2005**, *576*, 217.
[23] H.-F. Wang, X.-Q. Gong, Y.-L. Guo, Y. Guo, G. Z. Lu, P. Hu, *J. Phys. Chem. C* **2009**, *113*, 10229.
[24] H.-Y. Li, H.-F. Wang, X.-Q. Gong, Y.-L. Guo, Y. Guo, G. Z. Lu, P. Hu, *Phys. Rev. B* **2009**, *79*, 193401.
[25] M. V. Ganduglia-Pirovano, J. L. F. Da Silva, J. Sauer, *Phys. Rev. Lett.* **2009**, *102*, 026101.

